IEEE Access
Multidisciplinary | Rapid Review | Open Access Journal

Received February 24, 2019, accepted March 10, 2019, date of publication April 9, 2019, date of current version April 18, 2019.

Digital Object Identifier 10.1109/ACCESS.2019.2909756

Low-Speed Bearing Fault Diagnosis Based on ArSSAE Model Using Acoustic Emission and Vibration Signals

SYAHRIL RAMADHAN SAUFI[1,2], ZAIR ASRAR BIN AHMAD[1,2], MOHD SALMAN LEONG[1,2], AND MENG HEE LIM[2]

[1]Faculty of Engineering, School of Mechanical Engineering, Universiti Teknologi Malaysia, Johor Bahru 81310, Malaysia
[2]Institute of Noise and Vibration, Universiti Teknologi Malaysia, Kuala Lumpur 54100, Malaysia

Corresponding author: Syahril Ramadhan Saufi (msyahramadhan41@gmail.com)

This work was supported in part by the Institute of Noise and Vibration UTM under the Higher Institution Centre of Excellence (HICoE) under Grant R.K130000.7809.4J225, Grant R.K130000.7809.4J226, Grant R.K130000.7843.4J227, and Grant R.K130000.7843.4J228, in part by the UTM Research University under Grant Q.K130000.2543.11H36, and in part by the Fundamental Research Grant Scheme by The Ministry of Higher Education Malaysia under Grant R.K130000.7840.4F653.

ABSTRACT The development of rolling element bearing fault diagnosis systems has attracted a great deal of attention due to bearing components having a high tendency toward unexpected failures. However, under low-speed operating conditions, the diagnosis of bearing components remains a problem. In this paper, the adaptive resilient stacked sparse autoencoder (ArSSAE) is proposed to compensate for the shortcomings of conventional fault diagnosis systems at low speed. The efficiency of the proposed ArSSAE model is initially assessed using the CWRU database. Then, the proposed model is evaluated on actual vibration analysis (VA) and acoustic emission (AE) signals measured on a bearing test rig at low operating speeds (48–480 rpm). Overall, the analysis demonstrates that the ArSSAE model is able to perform an accurate diagnosis of bearing components under low-speed conditions.

INDEX TERMS Low speed, bearing fault diagnosis, vibration analysis, acoustic emission analysis, adaptive resilient stacked sparse autoencoder (ArSSAE).

I. INTRODUCTION

Rolling element bearings are commonly used in machinery such as excavators, stackers, swing shovels and steel mill cranes [1]. These machines are operated at low speeds due to their heavy weight and large structures. An unexpected failure of a heavy machinery bearing may result in an economic loss and lead to a long period of maintenance. Recently, many fault diagnosis systems have been focused on high-speed bearing fault diagnosis using vibration signal monitoring [2].

In order to prevent such failures, effective fault diagnosis systems for bearing components operating at low speeds require further development. Moustafa *et al.* wrote that an effective fault diagnosis system has been introduced for bearing components in high-speed conditions; however, fault diagnosis in low-speed operation still remains a difficult problem [3]. According to Caesarendra *et al.*, the range of low-speed operation is around 10–600 rpm [4]. The limitation of vibration analysis (VA) in low-speed operating machine fault diagnosis has led to the exploration of acoustic emission (AE) techniques [4], [5]. Caesarendra and Tjahjowidodo reported that the vibration signature produced at low speed is masked by a heavy background noise, which makes the signal more complex and makes it difficult to extract reliable features from the signal [6]. This is because the vibration signal is directly proportional to the acceleration of the vibrating component. However, Xiong *et al.* achieved satisfactory performance in diagnosing bearing conditions at a rotation speed of 230 rpm using EMD denoising and alpha-stable distribution [7]. In addition, Song *et al.* proposed a new signal feature extraction method for bearing conditions under low-speed operation [8].

AE techniques can be more sensitive than VA in detecting defects at low operating speed [9]. There are two conditions of the generation of AE signal, as mentioned in [4]. At high speed, the AE signal is generated based on the impact between the rolling element and the bearing raceway. Mean-

The associate editor coordinating the review of this manuscript and approving it for publication was Mu-Yen Chen.

while, at low speed, the transient elastic wave is generated based on the interaction of the rolling element and the bearing raceway. However, the AE signal is difficult to process due to the high sampling rate, typically up to 10 MHz [10]. Bechhoefer *et al.* conducted research on improving AE feature extraction [11]. The authors stated that the AE signal contains a large volume of data that must be processed, and the extracted AE features must be selected properly depending on the application (e.g., bearing or gear). The challenges and limitations of AE methods have been discussed by Sikorska and Mba [12]. Attempts to process the AE signal have been made by several researchers. For example, Van Hecke *et al.* resampled the AE signal using a heterodyne frequency reduction approach [13]. In addition, Ruiz-Cárcel *et al.* diagnosed bearing defects by using a spectral kurtosis diagram to enhance the fault features in AE signals [14]. In the past few decades, the AE burst detection system has been used in bearing fault diagnosis [15], [16]. This system could eliminate the difficulty of processing the continuous AE signal.

In recent years, deep learning models have been introduced to overcome the limitations of the traditional fault diagnosis system. The traditional system utilizes two common machine learning models: an artificial neural network (ANN) and a support vector machine (SVM). In general, it is necessary to properly extract and select features for ANN and SVM models so that they can be accurately classified [17]. The shallow architecture of traditional machine learning is only applicable for feature classification purposes [18]. In contrast, deep learning architecture is capable of extracting and designing the input data automatically using each layer of the deep network. This process could eliminate the need for manual feature extraction and feature selection, which are time-intensive. Liu *et al.* emphasized that deep learning outperforms any other traditional machine learning techniques in term of automated feature processing [19]. Deep learning techniques as applied to bearing fault diagnosis systems are rapidly being developed and it is able to deal with multiple types of input data as listed in Table 1. There are three types of input data that can be summarized from the literature analysis: statistical features, time domains and images of time-frequency transformation.

Among deep learning models, the stacked sparse autoencoder (SSAE) has shown promising performance in various applications such as medical imaging processing [20]–[22], speech recognition [23] and human activity recognition [24]. Several authors highlighted that SSAE performance is highly dependent on its architecture hyperparameter and human expertise is required to determine the exact values for hyperparameters or performance will suffer [25]–[27]. In addition, there is no standard procedure to determine the number of hidden nodes and layers in an SSAE network. At present, the SSAE's hyperparameter and hidden node number has been successfully optimized using metaheuristic algorithm as mentioned in the following research [28]. Wang *et al.* mentioned the effects of autoencoder hidden layer numbers on the model performance [29]. For example, Liu *et al.* used three hidden layers of SSAE network to diagnose bearing condition based on STFT image classification [30]. Ahmed *et al.* and Sun *et al.* stacked two layers of SAEs to extract a significant feature from a processed bearing signal [31], [32]. Chen and Li combined two hidden layers of SAEs and three hidden layers of DBNs so that a significant feature could be automatically extracted from the input data [33]. Meanwhile, Di and Wang discussed the varied prediction accuracies produced with different numbers of hidden layers [34].

TABLE 1. Application of deep learning model on different input data.

Authors	Method	Types of input data
Yang et al. [35]	Deep neural network	Frequency feature
Li et al. [36]	2DPCA and minimum distance method	Image of the frequency spectrum
Verstraete et al. [37]	Deep convolutional neural network	Image of time-frequency (STFT, Wavelet, HHT)
Li et al. [38]	Gaussian Bernoulli restricted Boltzmann machine	Time domain features
Haidong et al. [39]	Deep wavelet autoencoder with an extreme learning machine	1D Time domain
Chen et al. [40]	Deep neural network	Time domain features
Li et al. [41]	Fully-connected winner-take-all autoencoder	1D Time domain

In this paper, a novel method called an adaptive resilient stacked sparse autoencoder (ArSSAE) is proposed in order to deal with the aforementioned problems. The proposed model is applied to analyze three types of input data: time-frequency images, time domains and statistical features from VA and AE signals. The capability of the model to deal with the online dataset and experimental dataset has been studied.

The rest of the paper is organized as follows. Section II discusses the sparse autoencoder model and Section III describes improvements to it. Section IV discusses the preliminary analysis using the proposed model on the online database. Section V presents the experimental study on the bearing test rig. Sections VI and VII discuss the results and conclude the paper, respectively.

II. STRUCTURE OF STACKED SPARSE AUTOENCODER

An autoencoder network is based on a symmetrical three-layer network to learn high-level data representation. The model can be trained in an unsupervised manner.

The basic autoencoder network contains encoder and decoder functions. The hidden representation ($h \in R^k$) is mapped using the encoder function $h = f(w_1 x + b)$. The decoder function $\hat{x} = g(w_2 h + b)$ reconstructs the hidden representation to produce an output that has approximately equal characteristics to the original input. The loss function of an autoencoder is defined in Eq. 1:

$$J(W, b) = \frac{1}{2} \left\| h_{w,b}(x) - y \right\|^2, \tag{1}$$

where $J(W, b; x, y)$ represents the mean square error.

The sparse autoencoder (SAE) is another variant of autoencoder which enforces a constraint onto the hidden units to discover interesting features in the data [42]. The sparse autoencoder loss function is described in Eq. 2:

$$J_{sparse}(W, b) = J(W, b) + \beta \sum_{j=1}^{n} KL(\rho \| \hat{\rho}_j), \tag{2}$$

where $KL(\rho \| \hat{\rho}_j) = \rho \log \frac{\rho}{\hat{\rho}_j} + (1 - \rho) \log \frac{1-\rho}{1-\hat{\rho}_j}$ represents the sparsity penalty term, β is a weight of the sparsity penalty term, ρ is the sparsity parameter and $\hat{\rho}_j$ is the average activation of the hidden unit. The overall loss function of a stacked sparse autoencoder is shown in Eq. 3:

$$E = J_{sparse}(W, b) + J_{weight}(W, b), \tag{3}$$

where $J_{weight}(W, b) = \frac{\lambda}{2} \sum_{l=1}^{nl} \sum_{i}^{sl-1} \sum_{j}^{sl} \left(W_{ij}^{(l)} \right)^2$ is a weight decay term to prevent the network from overfitting.

The sparse autoencoder (SAE) network is stacked up to several numbers, and the softmax network is located on top of the stacking sparse autoencoder network. In this study, the combination of stacking SAE networks and softmax is called SSAE architecture, where the stacking of the SAE network represents the hidden layer of the whole network. Softmax is a classifier that aims to classify the features that were processed by the sparse autoencoder. The mathematical model of the softmax classifier is shown in Eq. (4):

$$h_\theta \left(x^i \right) = \begin{bmatrix} p(y^i = 1 | x^i; \theta) \\ p(y^i = 2 | x^i; \theta) \\ \cdot \\ \cdot \\ \cdot \\ p(y^i = k | x^i; \theta) \end{bmatrix} = \frac{1}{\sum_{i=1}^{k} e^{\theta_j^T x^i}} \begin{bmatrix} e^{\theta_1^T x^i} \\ e^{\theta_2^T x^i} \\ \cdot \\ \cdot \\ \cdot \\ e^{\theta_k^T x^i} \end{bmatrix}, \tag{4}$$

where $\theta_1, \theta_2, \ldots, \theta_k \in R^{n+1}$ are the model parameters and $1 / \sum_{i=1}^{k} e^{\theta_j^T x^i}$ normalizes the distribution to ensure that the sum is equal to one.

III. PROPOSED MODEL OF BEARING FAULT DIAGNOSIS SYSTEM

In this section, the proposed model is developed in order to deal with current problems as reported in the literature analysis. The first problem is that advance fault diagnosis systems for bearing fault diagnosis are limited under low-speed operating conditions. Second, several studies have found that AE outperforms vibration for monitoring bearing components at low operating speeds. However, a paper has been published on the application of vibration at an operating speed of 230 rpm where the fault diagnosis can be performed at low speed condition using vibration signal [7]. Third, there are three types of input data that can be fed into the deep learning model depending on the deep learning networks and machinery applications. Each type of input data (e.g. statistical features, time domains and images of time-frequency) will provide a different number of features. At present, each type of input data needs a different set of deep learning models, which require human intervention to manually change the architecture of the model depending on the input data characteristics. The performance of the machine learning model is heavily dependent on the quantity and quality of the features.

The modified architecture of the original autoencoder is constructed as illustrated in Fig. 1. The structure of the ArSSAE should have flexibility in processing any type of dataset in order to eliminate dependency on any particular feature extraction and feature selection methods. The developed model should also be robust and able to address the current problems of bearing fault diagnosis. First, the resilient back-propagation (Rprop) algorithm is implemented on the ArSSAE network to reduce the training time of the model Then, the ArSSAE hyperparameters (e.g., the number of hidden nodes, weight decay parameter λ, sparsity parameter ρ, and weight of sparsity penalty term β) are optimized using the differential evolution (DE) optimization method. Based on studies reviewed by Ab Wahab *et al.*, DE is among the best optimization methods [43]. The details of the DE and resilient algorithm implementation in the SSAE network can be referred to the following works [28]. To solve the hidden layer problem discussed in the preceding section, we developed a stacking layer of SAEs depending on the feature size as an initial reference configuration. However, the model may change the number of stacking layers if the initial hidden layer does not provide an accurate prediction. Determining the number of layers contained in a deep learning model is a problem that requires a trial and error process, and it is sometimes based on intuition. The common problems of deep learning models are computer processing load and time. The SSAE model suffers from two computational costs: i) computational processing for training the SSAE network and parameters (e.g. weight and bias); and ii) computational processing for optimizing the SSAE hyperparameters. Thus, we used DE and Rprop to reduce both costs by avoiding unnecessary computational processing, because the amount of computational processing required is directly proportional to the size of the network. The proposed model algorithm and flowchart are presented in Table 2 and Fig. 2 respectively.

A. DIFFERENTIAL EVOLUTION

In order to solve the hyperparameter selection problem discussed in the preceding section, DE is utilized to automate

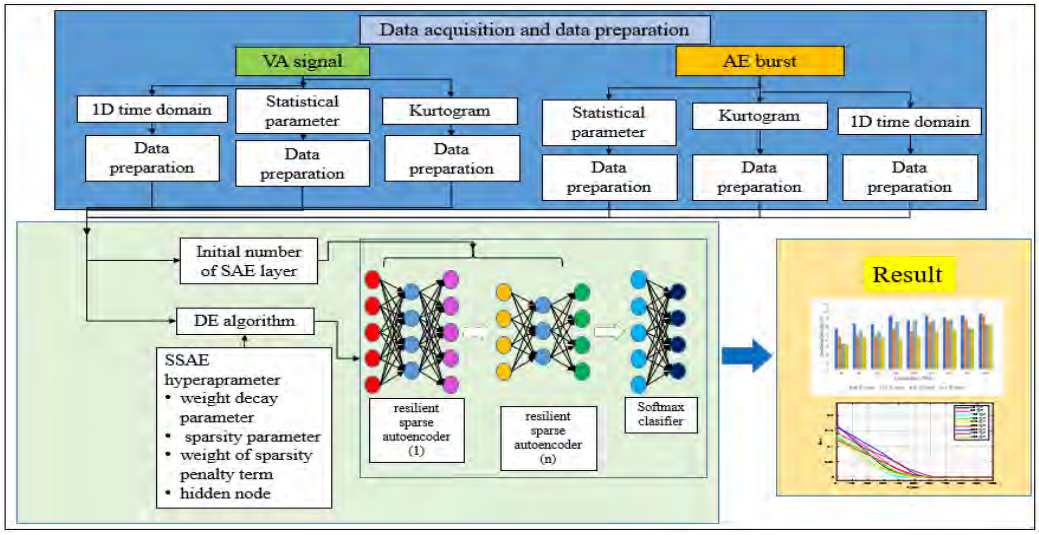

FIGURE 1. Proposed diagnosis system.

the process. The DE operator employs the sequence of mutation, crossover and selection. In addition, DE naturally alters its search behavior from exploration to exploitation as the population evolves due to its self-referential mutation. The selection process determines the vectors that will survive for the next generation.

In the mutation process, a mutant vector $V_{i,G}$ is generated by multiplying the amplification factor as in Eq. (4):

$$V_{i,G} = X_{r_1^i,G} + F.(X_{r_2^i,G} - X_{r_3^i,G}), \tag{5}$$

where $i = 1, \ldots, NP$, $r_1 r_2 r_3$ are random numbers, $r1 \neq r2 \neq r3 \neq i$, x is a decision vector and F is an amplification factor ([01]) that determines the differential variation of $(X_{r_2^i,G} - X_{r_3^i,G})$. The process continues with the crossover step. In the crossover operators, the offspring takes the probability $1 - Cr$ from the mutant vector $V_{i,G}$ of the current population X. The parent vector is combined with the mutated vector using Eqs. (6) and (7) to produce trial vector U:

$$U_{i,G+1} = \left(U_{1i,G+1}, U_{2i,G+1}, \ldots, U_{Di,G+1}\right) \tag{6}$$

and

$$U_{ji,G} \begin{cases} V_{ji,G+1} & if\ (rand_{i,j}[0,1] \leq Crorj = j_{rand}) \\ X_{ji,G} & otherwise. \end{cases} \tag{7}$$

where $j = \{1, 2, \ldots, D$, $Cr[0, 1]$ is the predefined crossover rate constant, $rand_{i,j}[0, 1]$ is the random number and $j_{rand}(1, 2, \ldots, D)$ is randomly chosen to ensure $U_{ji,G}$ gets at least one component from $V_{i,G}$.

The next step involves the selection process for choosing a vector between $(U_{i,G+1})$ and $(X_{ji,G})$ for the next generation $G + 1$. In an optimization problem, a vector with a higher fitness value is chosen using Eq. (8):

$$X_{i,G+1} = \begin{cases} U_{i,G} f\left(U_{i,G}\right) < f(X_{i,G+1}) \\ X_{i,G} f\left(U_{i,G}\right) \geq f(X_{i,G+1}). \end{cases} \tag{8}$$

In the DE algorithm, there are several control parameters, such as the scale factor F, the crossover rate Cr and the population number NP, that need to be set. Storn and Price recommended that the parameters should be [0.5,1], [0.8,1] and 10D for scale factor, crossover rate and population number respectively [44]. In this paper, the DE parameters are set as follows: $F = 0 : 8$, $Cr = 0 : 7$, $NP = 50$ and a maximum generation number $G_{\max} = 100$ is chosen as the termination criterion.

B. RESILIENT BACK-PROPAGATION ALGORITHM (RPROP)

The back-propagation algorithm updates the SSAE network parameters (e.g., weights and bias) in order to minimize the error function. Rprop has a faster speed of convergence and higher accuracy than other backpropagation algorithms [45]. It also has a different weight update routine compared to other methods. The algorithm updates the weight by considering the sign of the error gradient. The weight is updated via Eq. (9):

$$\Delta_{ij}(t) = \begin{cases} \eta^+ \Delta_{ij}(t-1), & if\ \dfrac{\delta E}{\delta w_{ij}}(t-1).\dfrac{\partial E}{\partial w_{ij}}(t) > 0 \\ \eta^- \Delta_{ij}(t-1), & if\ \dfrac{\delta E}{\delta w_{ij}}(t-1).\dfrac{\partial E}{\partial w_{ij}}(t) < 0 \\ \Delta w_{ij}(t-1), & otherwise. \end{cases} \tag{9}$$

The component Δ_{ij} is decreased by a factor of η^- when the partial derivative $\partial E/\partial w_{ij}$ changes its sign from one iteration to the next consecutive one. The component Δ_{ij} is increased by a factor of η^+ when the element of $\partial E/\partial w_{ij}$ maintains its sign from one iteration to the next consecutive iteration. In this study, the η^+ value is 1.2 while the η^- value is 0.5 as described in [46]. The weight will update its direction based

TABLE 2. The algorithm of ArSSAE model bearing specification.

Algorithm 1

Begin
Input data
Determine the no. of data sample (d), no. of features (f);
Set the number of SAE layer
If 1<f<512,
  Stacked 2 layers of SAE
else if 512≤f<1024,
  Stacked 3 layers of SAE
else 1024≤f<2048,
  Stacked 4 layers of SAE
Set the range of hidden node;
the range of hidden node for first hidden layer [lower limit: 300, upper limit: 350] with 75% reduction for the next consecutive hidden node of the SAE layer
DE algorithm:
  Set the hyperparameters range of each SAE layer;
Set the parameters of DE; Cr, F, NP, and Gmax
Initialise population $f(x), i = 1, \ldots, NP$
Evaluate the fitness of individual member D
Fitnessfunction: $error = (1 - \text{test classification accuracy}) \times 100$
while stopping criterion not satisfied **do**
for $i = 1, \ldots NP$ **do**
generate a new trial vector $U_{i,G+1}$
evaluate $f(U_{i,G+1})$
if $f(U_{i,G+1}) \leq f(x)$,
then $V_{i,G} = X_{r_1^i,G} + F.(X_{r_2^i,G} - X_{r_3^i,G})$
Else
$V_{i,G} = X_{i,G}$
end if
end for
for $i = 1, \ldots, NP$ **do**
Evaluate $V_{i,G}$
if $V_{i,G}$ better than D_i **then**
$D_i = V_{i,G}$
end if
end of
Save the best solution achieved so far
end while
Iteration reached with higher than 0% error
Update number of layer
Repeat the process
end

on Eq. (10):

$$\Delta w_{ij}(t) = \begin{cases} -\Delta_{ij}, & if \ \frac{\delta E}{\delta w_{ij}} > 0 \\ +\Delta_{ij}, & if \ \frac{\delta E}{\delta w_{ij}} < 0 \\ 0, & otherwise. \end{cases} \quad (10)$$

The details of the mathematical and algorithm explanation can be found in [46].

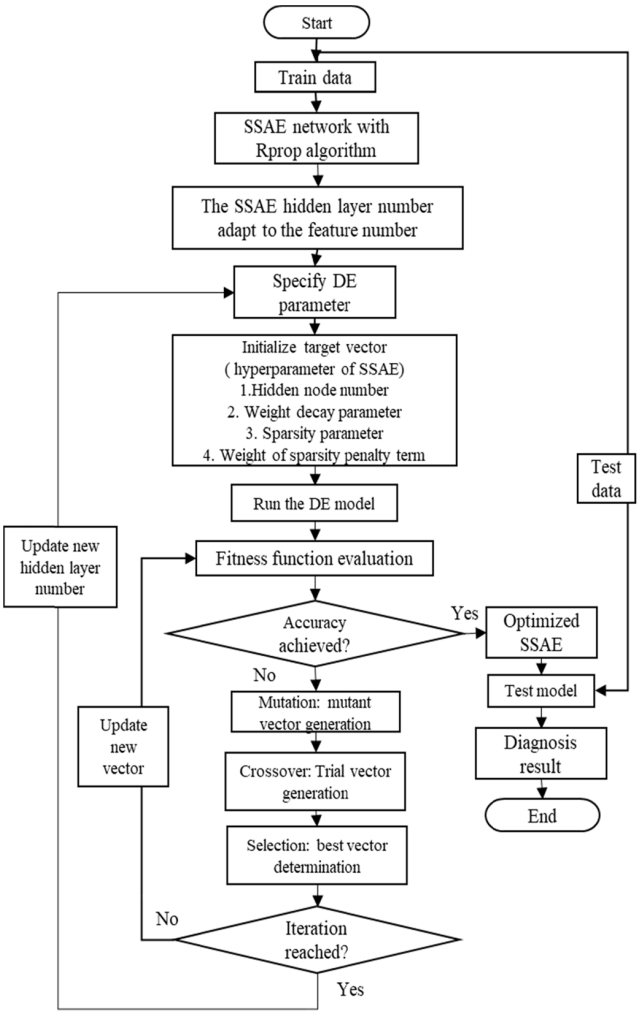

FIGURE 2. Flowchart of the adaptive SSAE model for bearing fault diagnosis.

IV. PRELIMINARY ANALYSIS OF PROPOSED MODEL USING BEARING ONLINE DATABASE (CWRU)

The proposed model was initially tested with a standard bearing database from Case Western Reserve University (CWRU) [47]. This data has been used by many researchers to test their proposed models of bearing fault diagnosis systems. Three types of datasets statistical features, time domains and kurtogram images were created from the vibration signal. The experimental setup is shown in Figure 3, and the data used in this study was recorded at a sampling rate of 48 kHz. We used the 1770–1800 rpm dataset with 10 different types of bearing conditions that contained three different fault severities (0.007-inch, 0.014-inch and 0.021-inch). The time domain was segmented using a length of 1600 data points for time domain data preparation. Ten statistical features—amplitude, root mean square, standard deviation, energy, kurtosis, skewness, crest factor, impulse factor, margin factor and shape factor—were extracted from the segmented time domain. For the third types of input data, the segmented signal was transformed into a kurtogram. Each of the bearing conditions

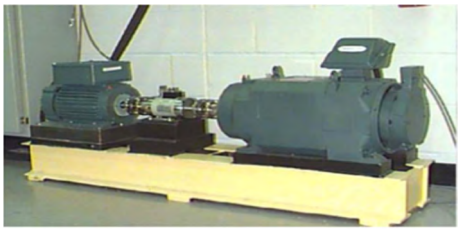

FIGURE 3. CWRU bearing testing platform.

TABLE 3. Optimization results of the proposed model based on the CWRU database.

Proposed model architecture / Input types	Number of features	Number of SAE layers	Number of hidden nodes	The testing result (%)
Statistical features	10	2 SAE layers	317 and 239	97.07
Time domain	1600	2 SAE layers	311 and 251	100
Kurtogram images	784	3 SAE layers	326,242 and 168	100

was sampled 100 times for training samples and 50 times for testing samples.

The analysis results are shown in Table 3. According to the results, the model achieved satisfactory performance on all types of datasets. The analysis proved that kurtograms can be used for bearing fault diagnosis. Typically, the analysis of time-frequency transformation relies on human interpretation to examine the fault characteristics. In this study, the kurtogram pattern was recognized based on the ArSSAE model. The ArSSAE demonstrated its effectiveness in mining the important features from the datasets. The number of SAE layers was initially calculated based on the feature boundary set in the algorithm. The model initially used four layers of SAE networks for time domain data. However, the model obtained the best classification prediction using two SAE layers. According to the results, the model achieved an accurate classification of statistical features and kurtogram images based on the initial hidden layer configuration. The classification result indicates that fault diagnosis using the proposed model is highly accurate.

V. EXPERIMENTAL SETUP

This section covers the experimental setup of the machinery fault simulator by Spectraquest. As illustrated in Fig. 4, the main components of the experimental rig include a $\frac{1}{2}$ horsepower (hp) motor, a motor controller and a rotor located on the middle of the shaft. A Rexnord link-belt ball bearing with Centric-Lok CL and Shurlok mounting collars were used for the duration of the experiment. The machine was operated at a range of low-speed operating conditions from 48 rpm (0.8 Hz) to 480 rpm (8 Hz). The AE sensor was placed near

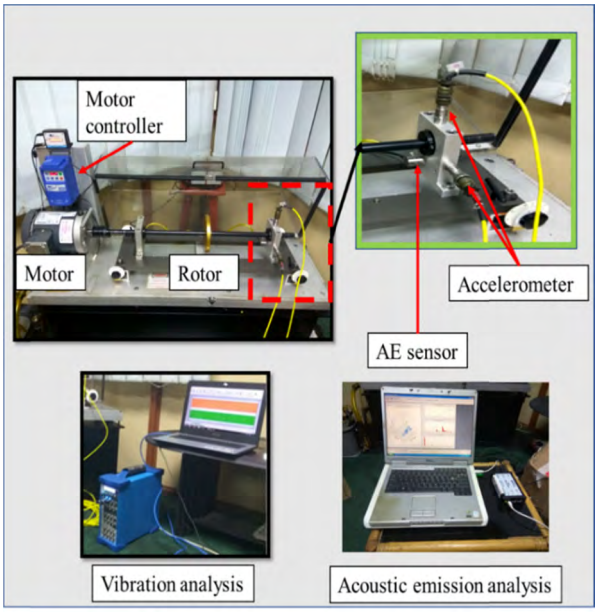

FIGURE 4. Experimental configurations.

the bearing housing and the accelerometer was located radially at the bearing housing. The AE instrumentation involved an AE sensor (PKWDI model) with an operating frequency range of 200–850 kHz, a single channel USB AE node and AEwin software. The AE system used in this research produced an AE burst waveform when the energy exceeded the threshold level. The setup of AE software acquisition was based on [48]. The AE hit bursts were obtained for a duration of 30 seconds.

The VA analysis involved two accelerometers, OROS data acquisition and NVgate software. The data was recorded in 30-second increments with a 25.6 kHz sampling rate. To simulate the bearing defect conditions, nine types of defects were introduced on the Rexnord bearing as shown in Fig. 5. Figs. 5(a), 5(b) and 5(c) represent the defects located on the outer race, inner race and ball bearing respectively. In addition, three types of combination defects were introduced on the bearing component: an outer race with inner race defect, an outer race with ball bearing defect and an inner race with ball bearing defect. For these, a defect size of 0.06 inches was used. The details of the bearing condition are illustrated in Table 4.

A. BEARING DEFECT FREQUENCY ANALYSIS

In order to validate the bearing conditions, the frequency spectrum of the defect was studied, and the result is shown in Fig. 6. The analysis of the frequency spectrum involves a rotation speed of 480 rpm and bearings with 0.06-inch defects. The calculation of bearing component defect frequency can be seen in Table 4. The defect frequency of inner race, outer race and ball are 39.6 Hz, 24.384 Hz and 30.384 Hz respectively. As can be seen in Fig. 6, the defect frequency of every bearing component is similar to the calculated frequency from the bearing defect equation.

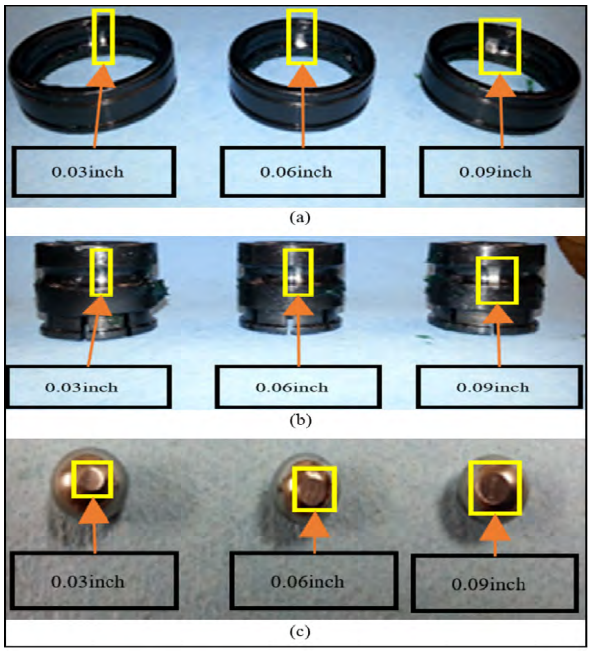

FIGURE 5. Bearing samples used in the experiment: a) outer race defect, b) inner race defect, and c) ball defect.

TABLE 4. Bearing specifications.

Bearing condition	Defect size (inch)	Shaft speed (rpm)	Specification
Normal	-	48 60 120 180 240 300 360 420 480	Ball number: 8 Ball diameter: 0.3125 inch Pitch diameter: 1.3189 inch BSF= 0.0332xcpm BDF= 0.0633xcpm BPFI= 0.0825xcpm BPFO= 0.0508xcpm
Outer race defect	0.03 0.06 0.09		
Ball defect	0.03 0.06 0.09		
Inner race defect	0.03 0.06 0.09		
Combination outer race and inner race defect	0.06		
Combination outer race and ball defect	0.06		
Combination inner race and ball defect	0.06		

Figs. 6(d), 6(e) and 6(f) show a spectrum of combination defect frequencies of inner with outer race, ball with inner race and ball with outer race respectively. Both amplitudes of the defect frequencies can be seen clearly on the spectrum. In summary, the analysis further proved that the defect was located at the right bearing component.

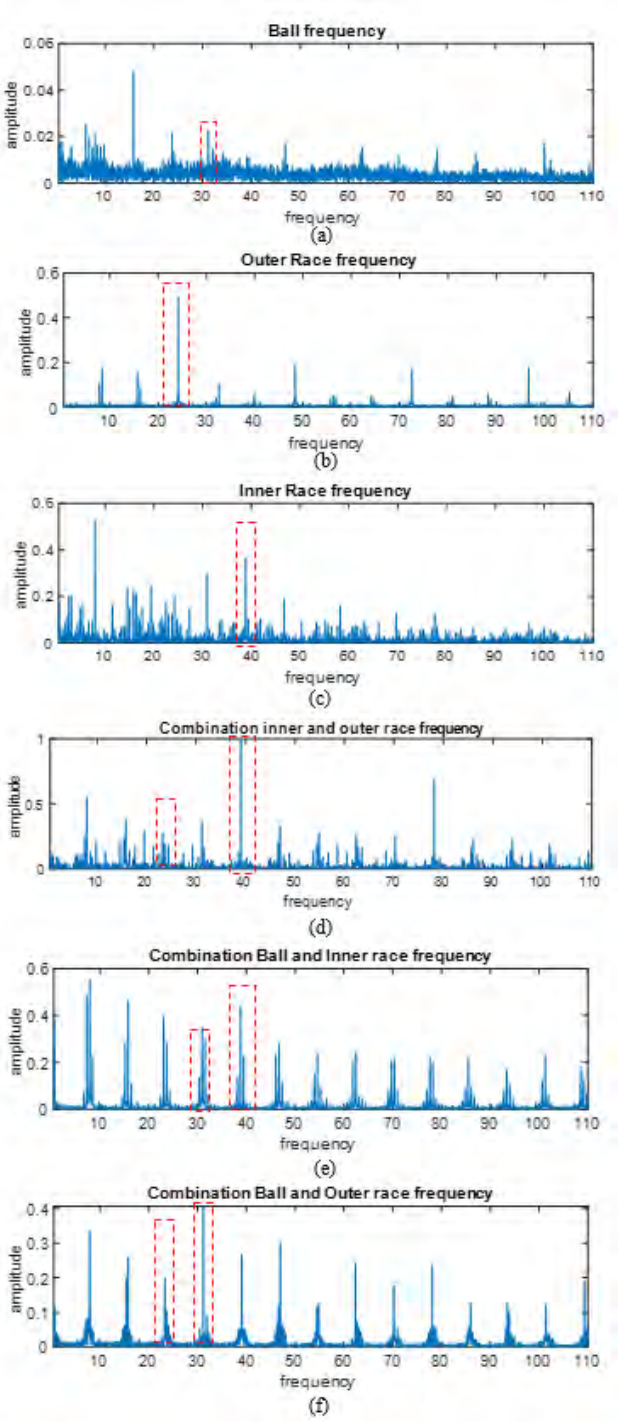

FIGURE 6. Bearing defect frequency.

B. DATA PREPARATION

In this study, six types of datasets were used to validate the proposed model: AE statistical features, AE kurtogram, AE burst waveforms (AE time domain), VA statistical features, VA kurtogram and VA segmented signals (VA time domain). The data preparation details are summarized in Table 5. For the first type of input data, the length of the AE and VA time domain represents the number

TABLE 5. Details of data preparation.

Input data	Feature number	Sample number
AE statistical features	11	Train: 1000 1300 Test: 500 650
AE time domain	1024	
AE kurtogram	784	
AE statistical features	10	
AE time domain	2025	
AE kurtogram	784	

of features. As mentioned in the preceding section, the AE system provided a burst signal with a length of 1024 data points. Meanwhile, the continuous VA signal was segmented into lengths of 2025 data points. Ten statistical features were extracted from the sliced VA signals including kurtosis, skewness, margin factor, impulse factor, crest factor and shape factor. Meanwhile, eleven statistical features were obtained from the AE system: amplitude, counts, duration, energy, absolute energy, signal strength, average signal level, rise time, root mean square, average frequency and counts to peak. Then, the AE burst and the segmented VA signal were transformed into kurtogram. The training dataset was sampled 100 times for each bearing condition, and the testing dataset was sampled 50 times for each bearing condition. Thus, 1000 and 1300 data samples represent the 10 and 13 classes training sets respectively, whereas 500 and 650 data samples represent the 10 and 13 classes testing sets.

VI. RESULTS AND DISCUSSION

The results of the experiments are presented in this section. In the first subsection, the comparative study of AE and VA signal features based on SVM model performance is discussed. The second subsection discusses the performance of the proposed model, the ArSSAE. In the last subsection, the comparative study between the proposed model and the SVM model is discussed.

A. COMPARATIVE STUDY OF AE AND VA STATISTICAL FEATURES BASED ON SVM MODEL PERFORMANCE

The initial analysis involved a comparative study between AE and VA statistical features using SVM models. Instead of performing a manual analysis of the statistical features, we used the SVM model to compare which signals provided more significant features. At first, the SVM model was analyzed with three dataset conditions: one set of 0.03-inch data (four classes), one set of 0.06-inch data (four classes) and one set of 0.09-inch data (four classes). For a four classes dataset, the SVM model is needed to diagnose the defect according to the location of the defect in the bearing component. Figs. 7 and 8 show the SVM classification accuracy for AE and VA statistical features respectively. The SVM model reached approximately 60 to 100% classification accuracy for 0.03-inch, 0.06-inch and 0.09-inch defects on AE signals.

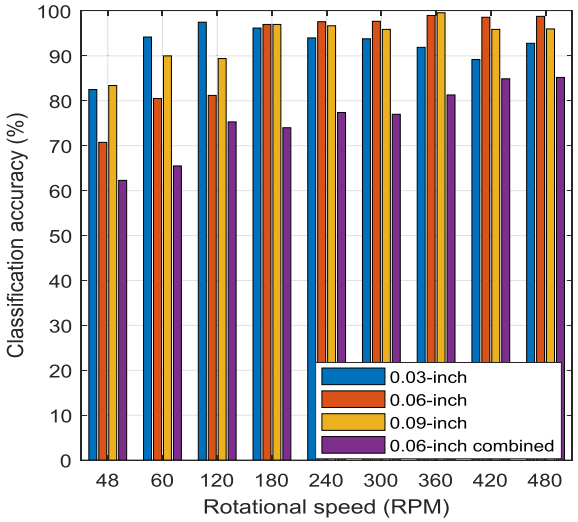

FIGURE 7. SVM result on AE statistical features.

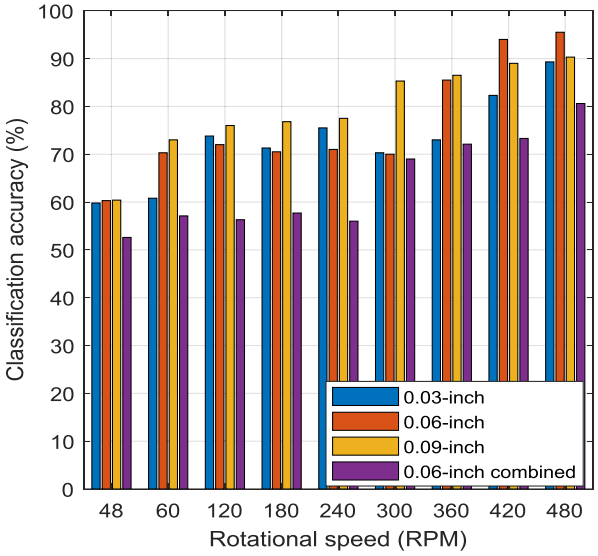

FIGURE 8. SVM result on VA statistical features.

Meanwhile, the model reached around 40 to 95% accuracy for VA signals. Next, the SVM was tested with the 0.06-inch combined dataset (seven classes), and the result is shown in Figs. 7–8 for both signals. The seven classes contained one normal bearing, three single defects and three combinations of defects. Classification accuracy was significantly greater using AE features than VA features when the rotational speed was less than 360 rpm. The SVM model was also evaluated on datasets representing 10 and 13 bearing fault conditions, and the result is shown in Fig. 9. The 10 classes dataset contained all defect conditions except combinations of defects. Meanwhile, the 13 classes dataset contained all available bearing conditions, as listed in Table 4. The SVM model produced higher classification accuracy on the AE signal's features compared to VA signal's features. It is worth mentioning that the performance of the SVM model increased when the rotational speed increased. Moreover, the

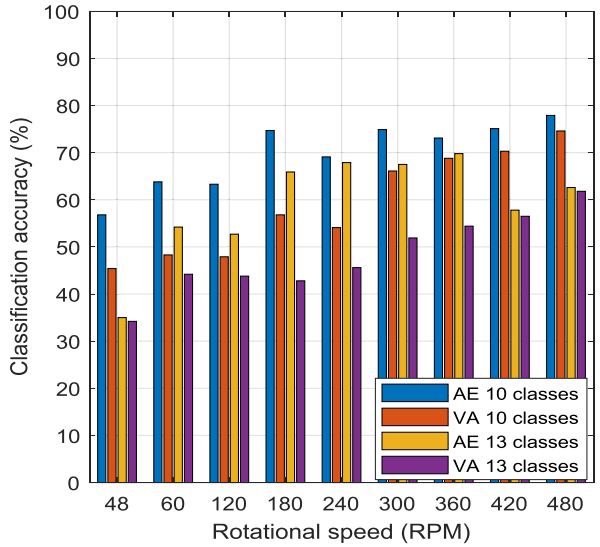

FIGURE 9. SVM classification on 10 and 13 classes.

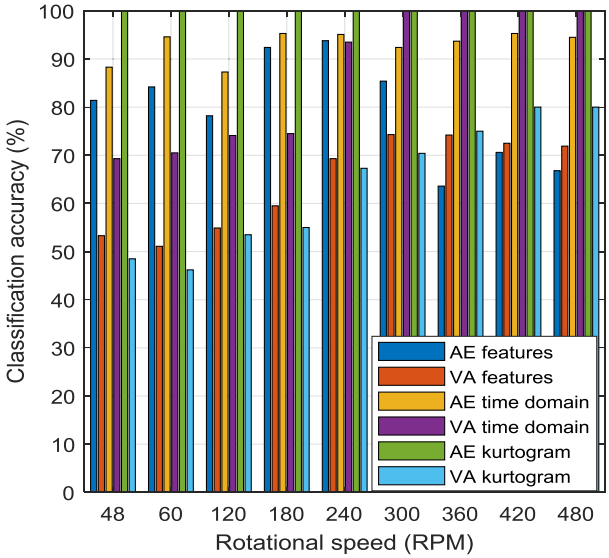

FIGURE 10. ArSSAE result between AE and VA analysis for 10 classes.

accuracy of the SVM model declined with an increase in the number of classes.

B. CLASSIFICATION PERFORMANCE OF THE PROPOSED MODEL (ArSSAE) ON AE AND VA SIGNALS FOR 10 and 13 CLASSES DATASETS

As discussed in the preceding analysis, the proposed ArSSAE model was developed based on multiple fault conditions. Therefore, the model was directly evaluated with the 10 and 13 classes datasets. It was fed with six types of datasets as listed in Table 5, and Fig. 10 shows the analysis result. For 10 classes, the defect location and defect severity can be simultaneously diagnosed. According to the assessment, the classification accuracy of the model depends on the type of input data. The model had higher performance on the

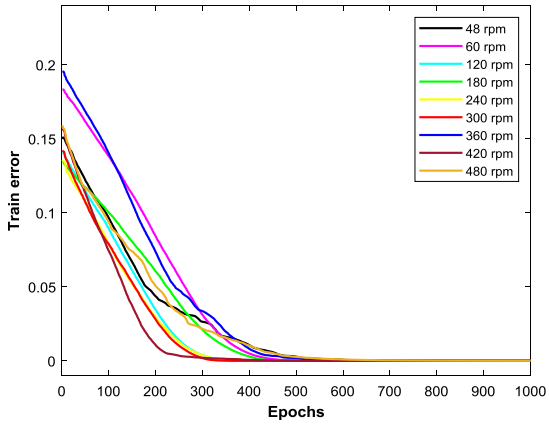

FIGURE 11. ArSSAE training performance on AE kurtogram (10 classes).

AE time domain compared to the VA time domain when rotational speed was less than 240 rpm, and it started to reach a satisfactory result on the VA time domain between 240 and 480 rpm. This demonstrates that the model can mine useful information from the time domain data. The fault diagnosis system based on the time domain is useful to eliminate the dependency on manual feature extraction from the time domain signal. According to the statistical feature results, the model had higher performance on AE than VA features at rotational speeds of 300 rpm and below. As the speed increased above 300 rpm, the performance using AE features was competitive with the performance using VA features. The classification accuracy of the model declined when using the vibration signal's kurtogram. The model produced the best classification accuracy on the AE kurtogram, where the model achieved 100% accuracy on all rotational speed datasets, even at the lowest speed. According to the model performance, the sample size used throughout the analysis is sufficient to provide the accurate classification prediction. By comparison, the model was more sensitive when using the AE signal's input data. It is believed that the performance of the model on vibration signals can be improved with the implementation of advanced signal processing techniques as discussed in [49]. By observation, the ArSSAE model produced a satisfactory performance on the AE kurtogram, AE time domain and VA time domain.

In order to demonstrate the performance of the model on the AE kurtogram, VA time domain and AE time domain, the training performance of the model is visualized as shown in Figs. 11, 12 and 13 respectively. The model has two major training processes, namely unsupervised pre-training and fine-tuning. The training plot is based on the best hyper-parameters selected by the DE algorithm. The analysis of AE kurtogram shows that the model required fewer than 700 epochs to reach 0% training error, and a consistent trend can be seen from the training plot. It can be observed that the model was only able to reach 0% training error at rotational speeds above 180 rpm when the model was trained using the VA time domain. The training performance of the model

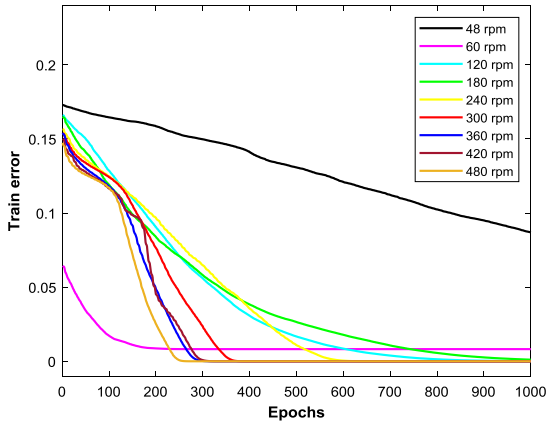

FIGURE 12. ArSSAE training performance on VA time domain (10 classes).

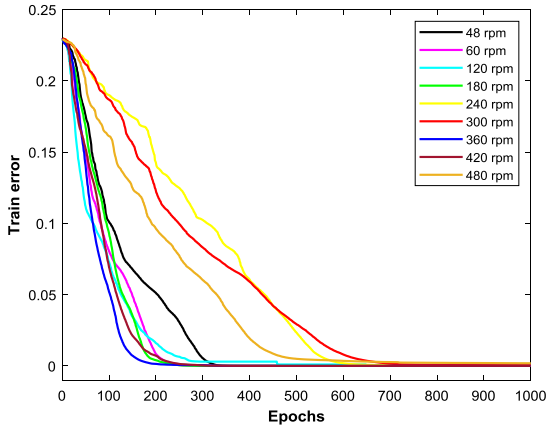

FIGURE 13. ArSSAE training performance on AE time domain (10 classes).

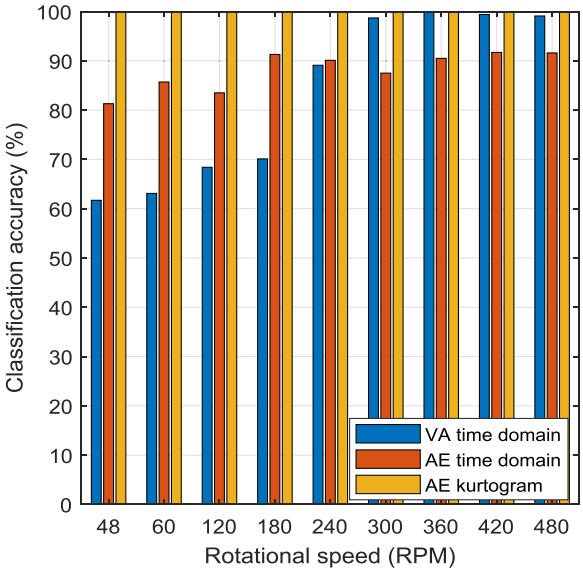

FIGURE 14. Performance of ArSSAE model on 13 classes datasets.

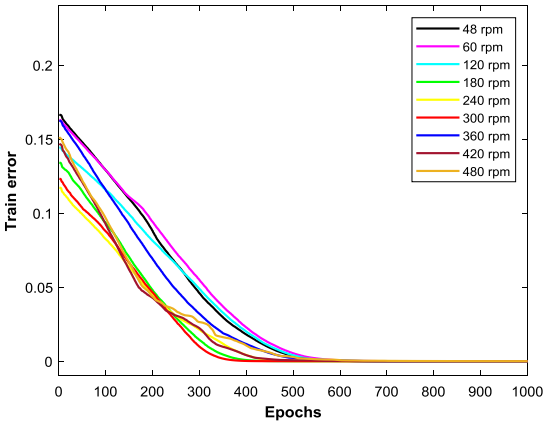

FIGURE 15. ArSSAE model training performance on AE kurtogram (13 classes).

on the AE time domain reached 0% training error on all rotational speeds, which proved that the model was capable of reaching a satisfactory performance during the testing phase. According to the training plot and the test accuracy produced by the model, the model did not suffer from overfitting problem during the analysis. The less accurate classification on several input data can be caused by the quality of the data where the model did not reach a satisfactory performance.

Subsequently, the ArSSAE model was evaluated with another bearing dataset that contained an additional set of three combination defect samples. Only AE kurtogram and VA and AE time domains were used because with those datasets, the ArSSAE model was capable of reaching a satisfactory classification prediction with 10 bearing fault conditions. The bearing's defect location, defect severity and defect combination can be simultaneously diagnosed using the 13 classes dataset. The result is shown in Fig. 14. It can be observed that there was no significant difference between the 10 and 13 classes results. According to the VA time domain result, the model started to reach a satisfactory performance at a rotational speed of 240 rpm, which is similar to the trend seen with the 10 classes dataset. The model's performance on both sets of time domain data slightly decreased with the 13 classes dataset. However, 100% classification accuracy was only achieved when the model was fed with the AE kurtogram dataset, even with the additional fault combinations. As can be seen, there was no reduction in model performance on the AE kurtogram, where the classification accuracy reached 100% for all rotational speeds. The fault diagnosis system based on image pattern recognition is quite new and requires further development so that it can be used for bearing prognosis.

To prove the superiority of the model on the 13 classes dataset, the training performance of the model on the AE kurtogram, VA and AE time domains is illustrated in Figs. 15, 16 and 17 respectively. The performance of the model at all rotational speeds was more consistent using the AE kurtogram compared to the AE and VA time domains. The model was unable to converge to the lowest training error at rotational speeds of 48 and 60 rpm using the VA time domain. The trend provides a helpful indicator of the model behavior

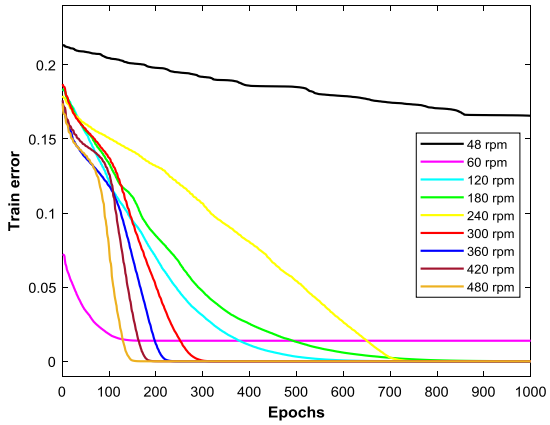

FIGURE 16. ArSSAE training performance on VA time domain (13 classes).

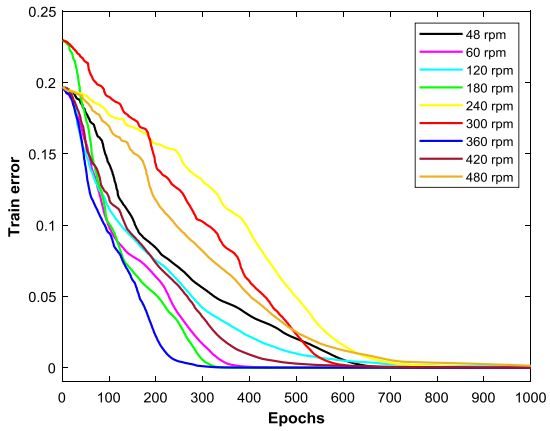

FIGURE 17. ArSSAE model training performance on AE time domain (13 classes).

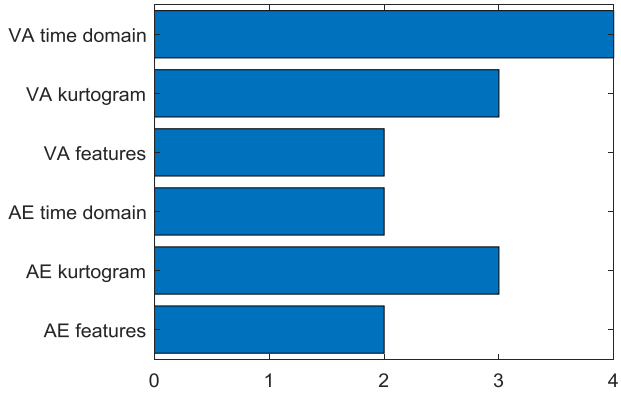

FIGURE 18. ArSSAE model configuration.

during the test analysis where the model did not suffer from overfitting.

Several factors may contribute to the increase in training time of the model including number of features, size of data samples, number of SAE layers in the ArSSAE network and training process of the DE algorithm. The number of SAE layers during the classification process is shown in Fig. 18, where it can be observed that the VA time domain data required the greatest number of SAE layers. In contrast, the model used only two layers of the SAE network to generalize the AE time domain, AE and VA features. The AE and VA kurtogram required three layers of the SAE network. Training time increases when more hidden layers are used; this problem has also been discussed by Wang *et al.* [42]. Instead of performing a manual iteration from a low hidden layer to a higher hidden layer, the hidden layer is initially set based on the size of the data feature, reducing the time required for manual iteration. The model reduces or increases the number of hidden layers if the initial hidden layer does not produce satisfactory classification accuracy. In addition, the optimization process for hyperparameter selection and hidden node numbers can eliminate the manual tuning process.

C. COMPARATIVE ANALYSIS BETWEEN ArSSAE MODEL AND SVM MODEL

Finally, the performance of the SVM and ArSSAE models was compared based on statistical features using the 10 classes dataset. The results for the ArSSAE and SVM models using VA statistical features were similar; the classification accuracy was around 50–75% and 40–75% respectively. Moreover, the classification accuracy of the ArSSAE was greater than that of the SVM when the models were fed with AE statistical features. The ArSSAE model was able to achieve classification accuracy as high as 94% using AE statistical features. Both models were observed to achieve greater accuracy on the AE signal's input data compared to the VA signal's input data. According to the analysis, accurate diagnosis on bearing components cannot be achieved by simply relying on statistical features, as the result produced is inconsistent and below a satisfactory diagnosis level. Therefore, the ArSSAE has an advantage over the SVM because the ArSSAE can be trained using another type of input data.

VII. CONCLUSIONS

In this research work, an intelligent bearing fault diagnosis system is proposed. The proposed model, called the adaptive resilient stacked sparse autoencoder (ArSSAE), was developed based on the flexibility of its architecture to change its network structure. The ArSSAE model offers several benefits. First, the model is based on a simple sparse autoencoder model that is easy to implement, and this model can work on any type of input dataset. Second, the model provides automated feature extraction and selection, which may reduce human involvement in selecting the best methods for both processes. Finally, the proposed model is able to deal with datasets that contain low numbers of features and data samples. The ArSSAE model works better on the AE kurtogram compared to other datasets in terms of training error and testing prediction.

According to the analysis, the ArSSAE model achieved the objective of the study: to develop a robust and flexible deep learning model that can be used for bearing fault diagnosis under low-speed operating conditions. The type of input data

plays an important role in accurate analysis, and input data types should be taken into consideration when performing fault diagnosis. The ArSSAE model's performance proved that fault diagnosis using vibration signals under low-speed operating conditions can be performed at speeds greater than 180 rpm.

REFERENCES

[1] W. Caesarendra, B. Kosasih, A. K. Tieu, and C. A. S. Moodie, "Application of the largest Lyapunov exponent algorithm for feature extraction in low speed slew bearing condition monitoring," *Mech. Syst. Signal Process.*, vols. 50–51, pp. 116–138, Jan. 2015.

[2] M. Cerrada *et al.*, "A review on data-driven fault severity assessment in rolling bearings," *Mech. Syst. Signal Process.*, vol. 99, pp. 169–196, Jan. 2018.

[3] W. Moustafa, O. Cousinard, F. Bolaers, K. Sghir, and J. P. Dron, "Low speed bearings fault detection and size estimation using instantaneous angular speed," *J. Vib. Control*, vol. 22, no. 15, pp. 3413–3425, 2016.

[4] W. Caesarendra, B. Kosasih, A. K. Tieu, H. Zhu, C. A. S. Moodie, and Q. Zhu, "Acoustic emission-based condition monitoring methods: Review and application for low speed slew bearing," *Mech. Syst. Signal Process.*, vols. 72–73, pp. 134–159, May 2016.

[5] T. R. Lin, E. Kim, and A. C. Tan, "A practical signal processing approach for condition monitoring of low speed machinery using peak-hold-down-sample algorithm," *Mech. Syst. Signal Process.*, vol. 36, no. 2, pp. 256–270, 2013.

[6] W. Caesarendra and T. Tjahjowidodo, "A review of feature extraction methods in vibration-based condition monitoring and its application for degradation trend estimation of low-speed slew bearing," *Machines*, vol. 5, no. 4, p. 21, 2017.

[7] Q. Xiong, Y. Xu, Y. Peng, W. Zhang, Y. Li, and L. Tang, "Low-speed rolling bearing fault diagnosis based on EMD denoising and parameter estimate with alpha stable distribution," *J. Mech. Sci. Technol.*, vol. 31, no. 4, pp. 1587–1601, 2017.

[8] L. Song, P. Chen, and H. Wang, "Vibration-based intelligent fault diagnosis for roller bearings in low-speed rotating machinery," *IEEE Trans. Instrum. Meas.*, vol. 67, no. 8, pp. 1887–1899, Aug. 2018.

[9] Y. Qu, D. He, J. Yoon, B. van Hecke, E. Bechhoefer, and J. Zhu, "Gearbox tooth cut fault diagnostics using acoustic emission and vibration sensors—A comparative study," *Sensors*, vol. 14, no. 1, pp. 1372–1393, 2014.

[10] Y. Qu, E. Bechhoefer, D. He, and J. Zhu, "A new acoustic emission sensor based gear fault detection approach," *Int. J. Prognostics Heal. Manage.*, vol. 4, pp. 32–45, Jul. 2013.

[11] E. Bechhoefer, Y. Qu, J. Zhu, and D. He, "Signal processing techniques to improve an acoustic emissions sensor," in *Proc. PHM*, 2013, pp. 1–8.

[12] J. Z. Sikorska and D. Mba, "Challenges and obstacles in the application of acoustic emission to process machinery," *Proc. Inst. Mech. Eng. E, J. Process Mech. Eng.*, vol. 222, no. 1, pp. 1–19, 2008.

[13] B. Van Hecke, J. Yoon, and D. He, "Low speed bearing fault diagnosis using acoustic emission sensors," *Appl. Acoust.*, vol. 105, pp. 35–44, Apr. 2016.

[14] C. Ruiz-Cárcel, E. Hernani-Ros, Y. Cao, and D. Mba, "Use of spectral kurtosis for improving signal to noise ratio of acoustic emission signal from defective bearings," *J. Failure Anal. Prevention*, vol. 14, no. 3, pp. 363–371, 2014.

[15] R. Unnþórsson, "Hit detection and determination in AE bursts," Acoustic Emission Research and Applications, Wojciech Sikorski, IntechOpen, Mar. 2013. doi: 10.5772/54754.

[16] S. M. Ali, K. H. Hui, L. M. Hee, and M. S. Leong, "Automated valve fault detection based on acoustic emission parameters and support vector machine," *Alexandria Eng. J.*, vol. 57, no. 1, pp. 491–498, 2018.

[17] Z. Liu, W. Guo, J. Hu, and W. Ma, "A hybrid intelligent multi-fault detection method for rotating machinery based on RSGWPT, KPCA and Twin SVM," *ISA Trans.*, vol. 66, pp. 249–261, Jan. 2017.

[18] K. H. Hui, C. S. Ooi, M. H. Lim, M. S. Leong, and S. M. Al-Obaidi, "An improved wrapper-based feature selection method for machinery fault diagnosis," *PLoS ONE*, vol. 12, no. 12, 2017, Art. no. e0189143.

[19] R. Liu, B. Yang, E. Zio, and X. Chen, "Artificial intelligence for fault diagnosis of rotating machinery: A review," *Mech. Syst. Signal Process.*, vol. 108, pp. 33–47, Aug. 2018.

[20] P. Cerveri, A. Belfatto, G. Baroni, and A. Manzotti, "Stacked sparse autoencoder networks and statistical shape models for automatic staging of distal femur trochlear dysplasia," *Int. J. Med. Robot. Comput. Assist. Surg.*, vol. 14, no. 6, p. e1947, 2018.

[21] P. He, P. Jia, S. Qiao, and S. Duan, "Self-taught learning based on sparse autoencoder for e-nose in wound infection detection," *Sensors*, vol. 17, no. 10, p. 2279, 2017.

[22] J. Xu, L. Xiang, R. Hang, and J. Wu, "Stacked sparse autoencoder (SSAE) based framework for nuclei patch classification on breast cancer histopathology," in *Proc. IEEE 11th Int. Symp. Biomed. Imag. (ISBI)*, Apr. 2014, pp. 999–1002.

[23] L. Deng, M. Seltzer, D. Yu, A. Acero, A.-R. Mohamed, and G. Hinton, "Binary coding of speech spectrograms using a deep auto-encoder," in *Proc. Interspeech*, Sep. 2010, pp. 1692–1695.

[24] B. Almaslukh, J. Almuhtadi, and A. Artoli, "An effective deep autoencoder approach for online smartphone-based human activity recognition," *Int. J. Comput. Sci. Netw. Secur.*, vol. 17, no. 4, pp. 160–165, 2017.

[25] M. Sohaib and J. M. Kim, "Reliable fault diagnosis of rotary machine bearings using a stacked sparse autoencoder-based deep neural network," *Shock Vib.*, vol. 2018, May 2018, Art. no. 2919637.

[26] G. B. Praveen, A. Agrawal, P. Sundaram, and S. Sardesai, "Ischemic stroke lesion segmentation using stacked sparse autoencoder," *Comput. Biol. Med.*, vol. 99, pp. 38–52, Aug. 2018.

[27] F. Ye, "Particle swarm optimization-based automatic parameter selection for deep neural networks and its applications in large-scale and high-dimensional data," *PLoS ONE*, vol. 12, no. 12, 2017, Art. no. e0188746.

[28] S. R. Saufi, Z. A. B. Ahmad, M. S. Leong, and M. H. Lim, "Differential evolution optimization for resilient stacked sparse autoencoder and its applications on bearing fault diagnosis," *Meas. Sci. Technol.*, vol. 29, no. 12, 2018, Art. no. 125002.

[29] F. Wang, B. Dun, G. Deng, H. Li, and Q. Han, "A deep neural network based on kernel function and auto-encoder for bearing fault diagnosis," in *Proc. IEEE Int. Instrum. Meas. Technol. Conf. (I2MTC)*, May 2018, pp. 1–6.

[30] H. Liu, L. Li, and J. Ma, "Rolling bearing fault diagnosis based on STFT-deep learning and sound signals," *Shock Vib.*, vol. 2016, Jul. 2016, Art. no. 6127479.

[31] H. O. A. Ahmed, M. L. D. Wong, and A. K. Nandi, "Intelligent condition monitoring method for bearing faults from highly compressed measurements using sparse over-complete features," *Mech. Syst. Signal Process.*, vol. 99, pp. 459–477, Jan. 2018.

[32] J. Sun, C. Yan, and J. Wen, "Intelligent bearing fault diagnosis method combining compressed data acquisition and deep learning," *IEEE Trans. Instrum. Meas.*, vol. 67, no. 1, pp. 185–195, Jan. 2018.

[33] Z. Chen and W. Li, "Multisensor feature fusion for bearing fault diagnosis using sparse autoencoder and deep belief network," *IEEE Trans. Instrum. Meas.*, vol. 66, no. 7, pp. 1693–1702, Jul. 2017.

[34] J. Di and L. Wang, "Application of improved deep auto-encoder network in rolling bearing fault diagnosis," *J. Comput. Commun.*, vol. 6, no. 7, pp. 41–53, 2018.

[35] Y. Yang, P. Fu, and Y. He, "Bearing fault automatic classification based on deep learning," *IEEE Access*, vol. 6, pp. 71540–71554, 2018.

[36] W. Li, M. Qiu, Z. Zhu, B. Wu, and G. Zhou, "Bearing fault diagnosis based on spectrum images of vibration signals," *Meas. Sci. Technol.*, vol. 27, no. 3, 2016, Art. no. 035005.

[37] D. Verstraete, A. Ferrada, E. L. Droguett, V. Meruane, and M. Modarres, "Deep learning enabled fault diagnosis using time-frequency image analysis of rolling element bearings," *Shock Vib.*, vol. 2017, Oct. 2017, Art. no. 5067651.

[38] C. Li, R. V. Sánchez, G. Zurita, M. Cerrada, and D. Cabrera, "Fault diagnosis for rotating machinery using vibration measurement deep statistical feature learning," *Sensors*, vol. 16, no. 6, p. 895, 2016.

[39] S. Haidong, J. Hongkai, L. Xingqiu, and W. Shuaipeng, "Intelligent fault diagnosis of rolling bearing using deep wavelet auto-encoder with extreme learning machine," *Knowl.-Based Syst.*, vol. 140, pp. 1–14, Jan. 2018.

[40] Z. Chen, S. Deng, X. Chen, C. Li, R.-V. Sanchez, and H. Qin, "Deep neural networks-based rolling bearing fault diagnosis," *Microelectron. Reliab.*, vol. 75, pp. 327–333, Aug. 2017.

[41] C. Li, W. Zhang, G. Peng, and S. Liu, "Bearing fault diagnosis using fully-connected winner-take-all autoencoder," *IEEE Access*, vol. 6, pp. 6103–6115, 2017.

[42] Y. Wang, M. Liu, Z. Bao, and S. Zhang, "Stacked sparse autoencoder with PCA and SVM for data-based line trip fault diagnosis in power systems," *Neural Comput. Appl.*, vol. 5, pp. 1–13, Apr. 2018.

[43] M. N. Ab Wahab, S. Nefti-Meziani, and A. Atyabi, "A comprehensive review of swarm optimization algorithms," *PLoS ONE*, vol. 10, no. 5, 2015, Art. no. e0122827.
[44] R. Storn and K. Price, "Differential evolution—A simple and efficient heuristic for global optimization over continuous spaces," *J. Global Optim.*, vol. 11, no. 4, pp. 341–359, 1997.
[45] N. Prasad, R. Singh, and S. P. Lal, "Comparison of back propagation and resilient propagation algorithm for spam classification," in *Proc. Int. Conf. Comput. Intell. Modeling Simulation*, Sep. 2013, pp. 29–34.
[46] M. Riedmiller and H. Braun, "A direct adaptive method for faster back-propagation learning: The RPROP algorithm," in *Proc. IEEE Int. Conf. Neural Netw.*, Mar. 1993, pp. 586–591.
[47] K. Loparo. Case Western Reserve University Bearing Data Center. Accessed: May 25, 2018. [Online]. Available: https://csegroups.case.edu/bearingdatacenter/pages/welcome-case-western-reserve-university-bearing-data-center-website
[48] B. Eftekharnejad, A. Addali, and D. Mba, "Defect source location of a natural defect on a high speed-rolling element bearing with acoustic emission," in *Proc. PHM*, 2011, pp. 1–7.
[49] F. Wang, C. Liu, W. Su, Z. Xue, H. Li, and Q. Han, "Condition monitoring and fault diagnosis methods for low-speed and heavy-load slewing bearings: A literature review," *J. Vibroeng.*, vol. 19, no. 5, pp. 3429–3444, 2017.

SYAHRIL RAMADHAN SAUFI is currently pursuing the Ph.D. degree with the Noise and Vibration Institute, Universiti Teknologi Malaysia, Kuala Lumpur, Malaysia. His current research interests include fault diagnosis, artificial intelligence, and structural assessment.

ZAIR ASRAR BIN AHMAD received the Ph.D. degree from the Faculty of Mechanical Engineering, Otto-von-Guericke-University Magdeburg, Magdeburg. He is currently a Senior Lecturer with the Faculty of Mechanical Engineering, Universiti Teknologi Malaysia, Skudai, Malaysia. His current research interests include civil engineering, acoustic engineering, and structural engineering.

MOHD SALMAN LEONG has more than 35 years professional engineering consulting experience, and is acknowledged by the industry and government agencies as the leading authority in acoustics, noise, and vibration in the country. He has been involved in many of the mega-projects and high impact consulting and investigation projects in oil and gas, power generation, infrastructure, and construction industries. He is currently a Professor, a Principal Consultant, and the Founding Director of the Institute of Noise and Vibration, Universiti Teknologi Malaysia, Kuala Lumpur, Malaysia.

MENG HEE LIM has more than 13 years professional consulting experience in acoustics and vibration, with specialization in machinery diagnostics. He has extensive experience in power generation gas and steam turbines, blade failures diagnostics, and experimental modal analysis. He is currently a Senior Lecturer and a Consultant with the Noise and Vibration Institute, Universiti Teknologi Malaysia, Kuala Lumpur, Malaysia.